

A Structural and Morphological Study of $\text{LiCo}_{1-x}\text{Sm}_x\text{O}_y$ Powders Obtained by the Sol-Gel Method

Víctor H. Colín Calderón¹, Antonieta García Murillo^{1*}, Felipe de Jesus Carrillo Romo¹, Arturo Cervantes Tobón²

¹Instituto Politécnico Nacional CIITEC, Cerrada de Cecati s/n, Azcapotzalco, Santa Catarina, México

²Instituto Politécnico Nacional-ESIQIE, Av. Instituto Politécnico Nacional s/n., Mexico City, México

Email: *angarciam@ipn.mx

How to cite this paper: Calderón, V.H.C., Murillo, A.G., de Jesus Carrillo Romo, F. and Tobón, A.C. (2022) A Structural and Morphological Study of $\text{LiCo}_{1-x}\text{Sm}_x\text{O}_y$ Powders Obtained by the Sol-Gel Method. *Advances in Nanoparticles*, 11, 1-12.
<https://doi.org/10.4236/anp.2022.111001>

Received: December 16, 2021

Accepted: January 27, 2022

Published: January 30, 2022

Copyright © 2022 by author(s) and Scientific Research Publishing Inc. This work is licensed under the Creative Commons Attribution International License (CC BY 4.0).

<http://creativecommons.org/licenses/by/4.0/>



Open Access

Abstract

In this study, the synthesis of $\text{LiCo}_{1-x}\text{Sm}_x\text{O}_y$ powders ($X = 0.002, 0.004, 0.006, 0.008, \text{ and } 0.1$) by the sol-gel method and the influence of Sm on their structural and morphological properties is reported for the first time. The results of x-ray diffraction (XRD) studies show that LiCoO_2 powders synthesized at temperatures up to 700°C present a characteristic hexagonal crystalline phase of the $\alpha\text{-NaFeO}_2$ type (space group R-3m), revealing a shift in the (0 0 3) Bragg reflection, which reflects the presence of Sm in the crystalline structure. The morphology was spheroidal and, on average, 122 nm in size. Based on the data obtained, $\text{LiCo}_{1-x}\text{Sm}_x\text{O}_y$ powders ($X = 0.002, 0.004, 0.006, 0.008, \text{ and } 0.1$) show promise as a material for use in the cathodes of lithium-ion batteries.

Keywords

Cathode, Batteries, Samarium, Sol-Gel, Nanoparticles

1. Introduction

The portability of electrical energy is a fundamental part of our daily life, [1] due to the applications of this energy in devices such as cell phones, tablets, laptops, and hybrid, and electric cars. Nowadays, these devices require greater efficiency from batteries [2]. There are numerous reports from studies that have been done on the development of new materials that could improve volumetric and gravimetric properties of batteries [3].

Since their commercialization in the 1990s, LiCoO_2 cathodes have been a con-

ventional component of lithium-ion batteries, [4] [5] [6] due to their high electrical capacity and their electrochemical stability [7] [8]. They have been widely used to enhance electrochemical properties and to provide electrical solutions in response to a growing demand for electrical portability [8] [9] [10].

Researchers have proposed two methods for improving the performance of LiCoO₂ cathodes [1] [11]. The first is to introduce different doping metals into the matrix (Fe, Cr, and M) [12]; the second is to coat the cathode with different metal oxides (such as Al₂O₃, B₂O₃, and TiO₂) [13]. Although researchers have focused on using certain groups of chemical elements, they have neglected rare earths, which have been shown to have properties that could be key to overcoming technological challenges [4] [11].

In 2007, Yanhuai *et al.* reported on the doping effects of Re = lanthanum, cerium, and praseodymium in Li [Ni_{1/3}Co_{1/3}Mn_{1/3}]_{1-x}Re_xO₂ cathodes, showing that the cathode matrix can be doped with rare earths, provoking a distortion of the crystalline structure at a maximum doping level of lanthanum at 0.03 mol%. The optimization of the cathode's electrochemical properties was related to crystal deformation of LiNi_{1/3}Co_{1/3}Mn_{1/3}O₂ which increased the cell parameters and enabled the lithium ions to diffuse [14].

The structural stability of a Sm 0.01 mol%-doped LiNi_{0.5}Mn_{1.5}O₄ cathode was reported in 2014 by Mingyue Mo *et al.* [15]; this low content of Sm in the cathode favored the conductivity of the lithium ion. In 2016, Xudong Meng *et al.* [16] increased the charge retention capacity of the LiFePO₄/C cathode by 96%, following doping with Sm at 6 mol%; this study revealed that samarium ions increase the conductivity and diffusion of lithium ions, improving their electrochemical performances and, as a result, their charge retention capacity.

The inclusion of rare earth elements in Li cathodes is an alternative to satisfy the real high energy source requirements. Therefore, to the best of our knowledge, in order to determine the effects of Sm on the structural and morphological properties of LiCoO₂, the system LiCo_{1-x}Sm_xO_y reported in this study was synthesized by the sol-gel method, for the first time. The characteristics of the Sm-doped powders obtained were structurally and morphologically compared with a non-doped system.

2. Experimental Procedure

2.1. Synthesis of Powders

LiCoO₂ and LiCo_{1-x}Sm_xO_y powders ($X = 0.002, 0.004, 0.006, 0.008$ and 0.01) were prepared by the sol-gel method. The synthesis procedure was as follows: 22 mmol of lithium nitrate (LiNO₃; Sigma Aldrich) was mixed with 20 ml of distilled water. After 20 min of constant stirring, 20 mmol of cobalt nitrate (Co (NO₃)₃ 8H₂O; ≥98% Sigma Aldrich) were added to the solution and magnetically stirred for 40 min to synthesize non-doped LiCoO₂ powders. Then an appropriate quantity of samarium nitrate (Sm (NO₃)₃ 8H₂O; 99.9% Aldrich) ($X = 0.002, 0.004, 0.006, 0.008,$ and 0.01) was incorporated into the non-doped precursor solution to produce a LiCo_{1-x}Sm_xO_y-doped precursor solution. A second solution

was prepared as follows: 0.219 mmol of citric acid ($\text{HOC}(\text{CO}_2\text{H})(\text{CH}_2\text{CO}_2\text{H})_2$, H_2O ; $\geq 99.0\%$ Sigma Aldrich) was dissolved in 5 ml of distilled water for 20 minutes, and this second solution was then added to the $\text{LiCo}_{1-x}\text{Sm}_x\text{O}_y$ -doped precursor solution. After a 140°C drying treatment for 2 hours, non-doped and Sm-doped gels were obtained. The resulting powders were heat-treated at 700°C for 24 hours, to yield LiCoO_2 and $\text{LiCo}_{1-x}\text{Sm}_x\text{O}_y$ crystalline powders.

2.2. Characterization of Powders

Both powders, the non-doped LiCoO_2 and the doped $\text{LiCo}_{1-x}\text{Sm}_x\text{O}_y$ ($X = 0.002, 0.004, 0.006, 0.008, \text{ and } 0.01$) were labeled as shown in **Table 1**. The crystalline structure of the powders was studied using a Bruker eco D8 Advance diffractometer with $\text{K}_{\alpha 1}$ radiation, with a Cu-K_{α} radiation source ($\lambda = 1.5406$), and 2θ values ranging from 10° to 80° , with a step size of $0.02^\circ \text{ s}^{-1}$. The morphological observations were carried out using a scanning electron microscope (JEOL JSM-6390LV) operated at 15 kV.

3. Results and Discussion

3.1. Structural Properties

The x-ray diffraction patterns obtained from the $\text{LiCo}_{1-x}\text{Sm}_x\text{O}_y$ powders ($X = 0.002, 0.004, 0.006, 0.008, \text{ and } 0.01$) (see **Table 1**), heat-treated at 700°C , are shown in **Figure 1(a)**.

These powders exhibit a rhombohedral crystalline structure (ICSD 98-004-8103) characteristic of LiCoO_2 [17] [18] [19] with no secondary phases. The space group associated with this structure is R-3m (166), known as a high-temperature structure, or HT- LiCoO_2 [20]; it is formed of alternating cobalt and lithium layers with oxygen anions, as reported by Bruno *et al.* [21]; a schema of this structure is shown in **Figure 1(b)**.

The rhombohedral structure obtained corresponds to the $\alpha\text{-NaFeO}_2$ type [18] [19]. The LT- LiCoO_2 to HT- LiCoO_2 transformation was caused by the distortion of the face-centered cubic structure (FCC) along the cell parameter c , manifesting itself in a clear separation of the crystalline planes (006) and (012), which are found between 35° and 40° , and planes (018) and (110), located between 65° and 70° [17] [19] [22] (see **Figure 1(a)**). Another indicator of hexagonal crystallization is the high intensity of planes (003) and (004), which demonstrates that the desired HT- LiCoO_2 structure was obtained [20] [23].

The shift in the Bragg peaks was analyzed focusing on plane (003) (see **Figure 2(a)**). The $2\text{-}\theta$ degree shifts in the samples were ascertained and compared. The

Table 1. Terms used and different Sm concentrations of the $\text{LiCo}_{1-x}\text{Sm}_x\text{O}_y$ powders.

LiCo _{1-x} Sm _x O _y powders					
Sample name	LiCo _{0.998} Sm _{0.002} O ₂	LiCo _{0.996} Sm _{0.004} O ₂	LiCo _{0.994} Sm _{0.006} O ₂	LiCo _{0.992} Sm _{0.008} O ₂	LiCo _{0.99} Sm _{0.01} O ₂
	Sm 0.2 mol%	Sm 0.4 mol%	Sm 0.6 mol %	Sm 0.8 mol %	Sm 1 mol %

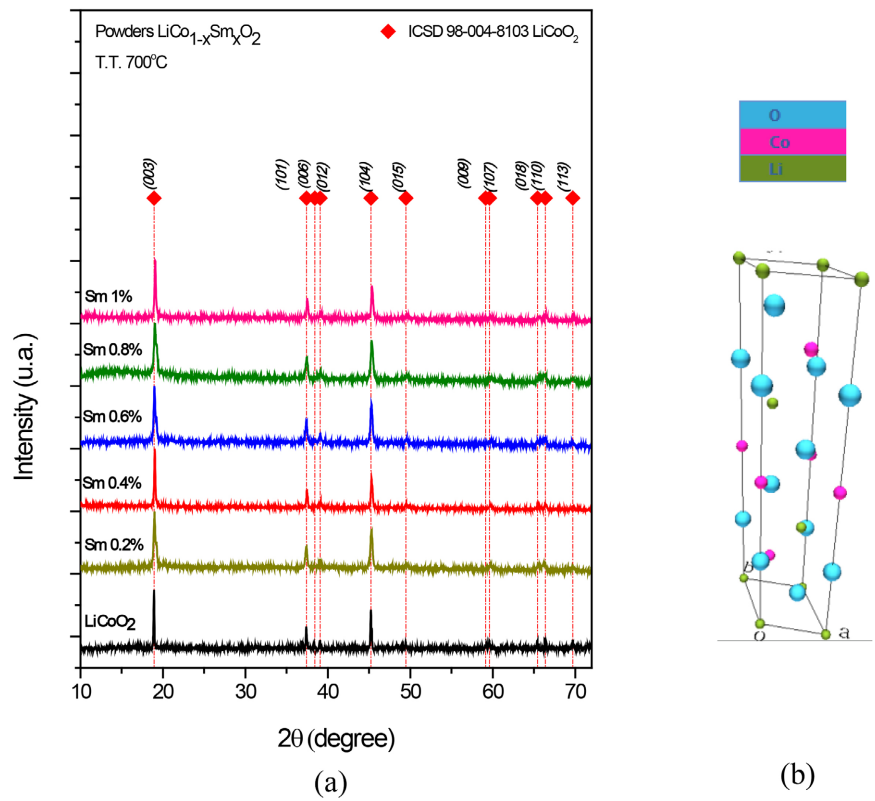


Figure 1. (a) XRD pattern and (b) scheme of the rhombohedral structure.

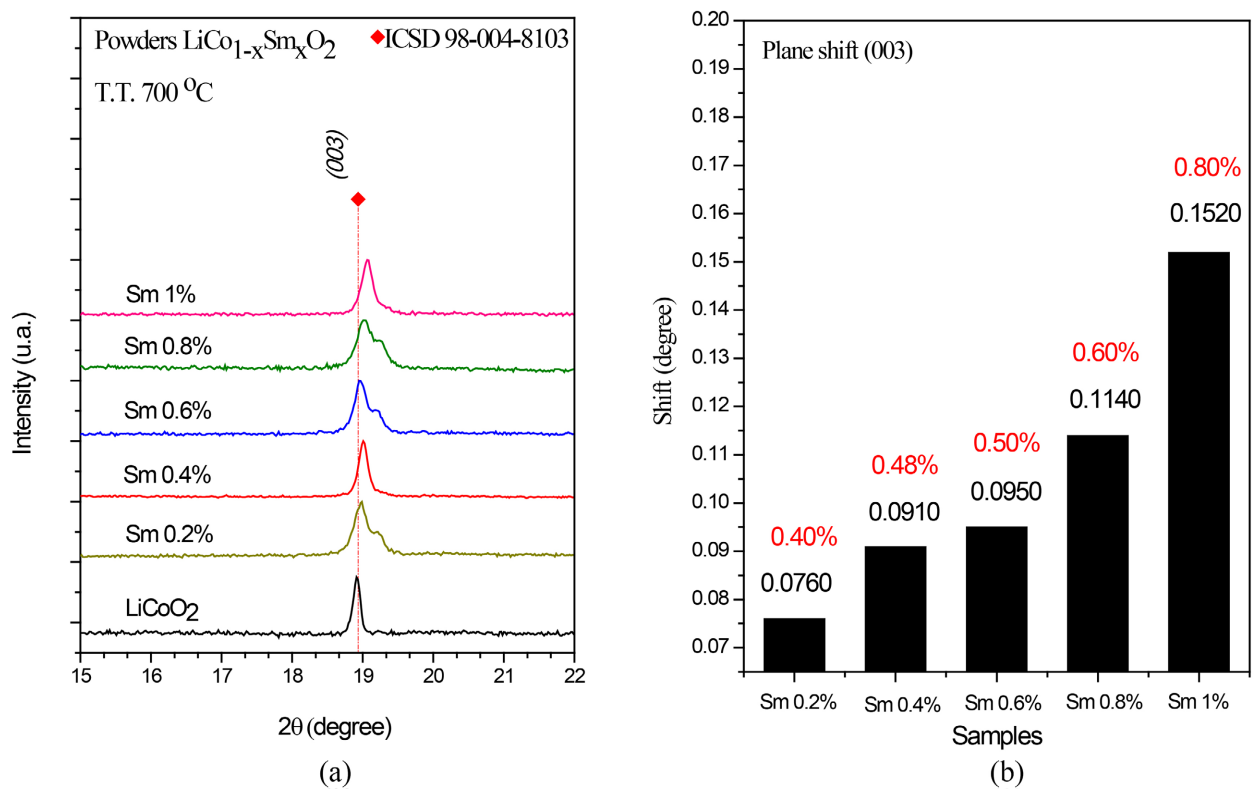


Figure 2. (a) XRD patterns of Sm doped $\text{LiCo}_{1-x}\text{Sm}_x\text{O}_2$ powders heat-treated at 700°C ; (b) 2θ values shift of (0 0 3) hkl Bragg reflection.

2θ shift in values between the non-doped powders (LiCoO_2) and the Sm-co-doped ones ($\text{Sm} = 0.002, 0.004, 0.006, 0.008, \text{ and } 0.1$) was 0.11° . The data obtained are summarized in **Table 2**. **Figure 2(b)** shows the increases in degree as the samarium concentration increases to 1 mol%.

To demonstrate the distortion of cell parameters, Rietveld refinement was performed on all the synthesized samples, yielding acceptable confidence values (GOF). The results are shown in **Table 3**.

Figure 3 illustrates the dimensional changes in cell parameters a , b , and c of the rhombohedral structure. The black line indicates a size increase of 0.0134 \AA in parameters a and b ; shown in red is an increase in cell parameter c , equal to 0.0183 \AA .

By increasing the concentration of Sm in the LiCoO_2 crystalline structure, the cell parameters increase (**Figure 3**). This is due to Sm^{3+} , which has an ionic radius of 1.09 \AA [24] [25], greater than that of Co, at 0.545 \AA [26], and which provokes a distorted crystalline structure.

Table 2. 2θ values of (0 0 3) hkl Bragg reflection of $\text{LiCo}_{1-x}\text{Sm}_x\text{O}_y$ powders.

hkl (0 0 3)	LiCoO_2	Sm 0.2%	Sm 0.4%	Sm 0.6%	Sm 0.8%	Sm 1%
Initial position (degree)	18.911	18.987	19.002	19.006	19.025	19.063
Shift (degree)		0.0760	0.0910	0.0950	0.1140	0.1520

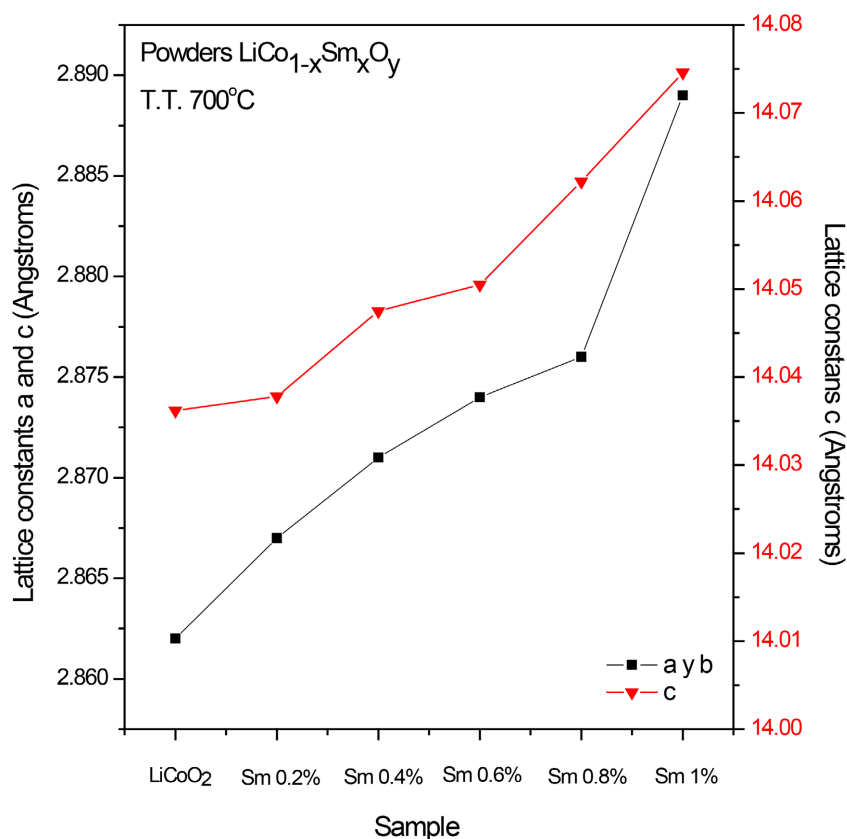


Figure 3. Lattice constants $a = b$ and c for samples heat-treated at 700°C .

This distortion of the unit cell enables lithium ions to migrate and thereby improves the electrochemical reactions [24]. The integrated intensity ratio between the (003) and (004) Bragg reflections (see **Figure 4**) indicates the degree of cation order in the LiCoO_2 [27] [28] structure. A value of $I(003)/I(104)$ higher than 1.2 promises to improve electrochemical performances of the cathode materials [27] [29]. **Table 3** shows the values obtained from the integrated intensities corresponding to the LiCoO_2 Sm 0.2%, Sm 0.4%, Sm 0.6%, Sm 0.8% y Sm 1% powders. The values for each sample are higher than 1.2, with the highest value corresponding to the sample doped with Sm at 0.1, equal to 1.54. This suggests that the alternating layers of Co and O allowed lithium ions to diffuse during the charge/discharge process.

Crystallite size was estimated using the Scherrer equation (Equation (1)), where $k = 0.9$, $\lambda = \text{wavelength}$ (1.5418 Å), $\beta = \text{FWHM}$, and $\Theta = \text{the Bragg angle}$ [30] [31]. The average size of the LiCoO_2 , Sm 0.2%, Sm 0.4%, Sm 0.6%, Sm 0.8% y Sm 1% was 30 nm (see **Figure 5**). The smallest crystallite (24 nm) was observed for the Sm 0.8 mol%-doped powder, and in the samples, the size increased up to 36 nm for the Sm 1 mol% sample.

$$D_{hkl} = \frac{k\beta}{\beta \cos \theta} \lambda \quad (1)$$

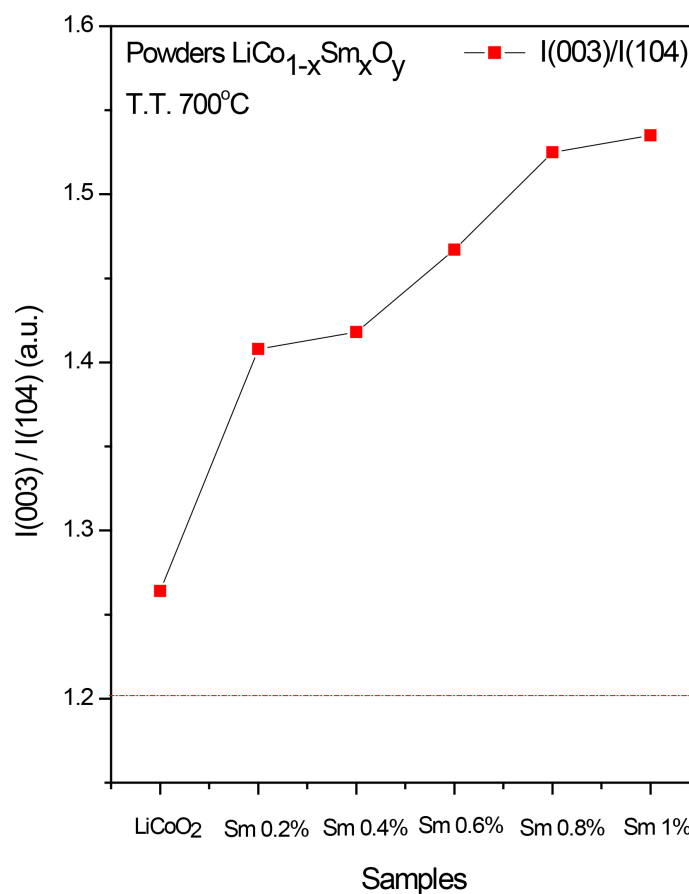
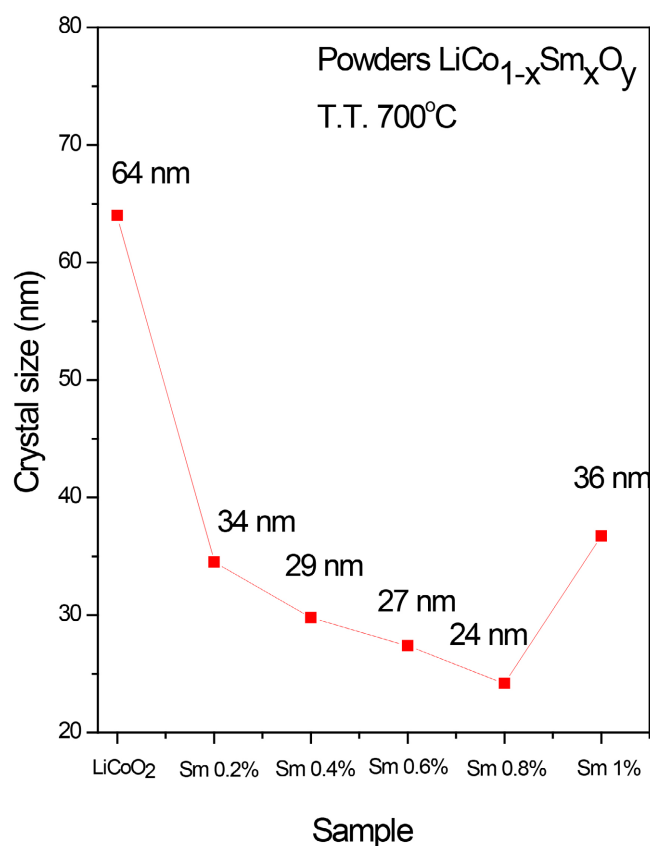


Figure 4. $I(003)/I(004)$ ratios of the $\text{LiCo}_{1-x}\text{Sm}_x\text{O}_y$ powders.

Table 3. Lattice constants and I(003)/(004) ratios for different $\text{LiCo}_{1-x}\text{Sm}_x\text{O}_y$ powders.

Sample	Lattice constants				Gof	I(003)/I(004)
	$a\gamma b$ (Å)	c (Å)	$\alpha\gamma\beta$	γ		
LiCoO ₂	2.868	14.028	90°	120°	0.93	1.26
Sm 0.2%	2.867	14.0378	90°	120°	1.19	1.40
Sm 0.4%	2.871	14.0475	90°	120°	1.09	1.41
Sm 0.6%	2.874	14.0505	90°	120°	1.24	1.46
Sm 0.8%	2.876	14.0622	90°	120°	1.5	1.53
Sm 1%	2.889	14.0746	90°	120°	0.85	1.54

**Figure 5.** Crystallite size for Sm doped $\text{LiCo}_{1-x}\text{Sm}_x\text{O}_y$ powders.

3.2. Morphological Results

Figure 6 shows the micrographs obtained by scanning electron microscopy (SEM) for the powders prepared by the sol-gel method, doped at concentrations of Sm 0.2%, Sm 0.4%, Sm 0.6%, Sm 0.8% y Sm 1%, and for the non-doped LiCoO₂ system.

Figure 6(a) shows the morphology of the LiCoO₂; it is a well-rounded morphology with a particle size of approximately 136 nm. Adding citric acid during the synthesis process generates smaller particles, depending on the citric acid/metal ratio, as reported by Wein-duo *et al.* [17].

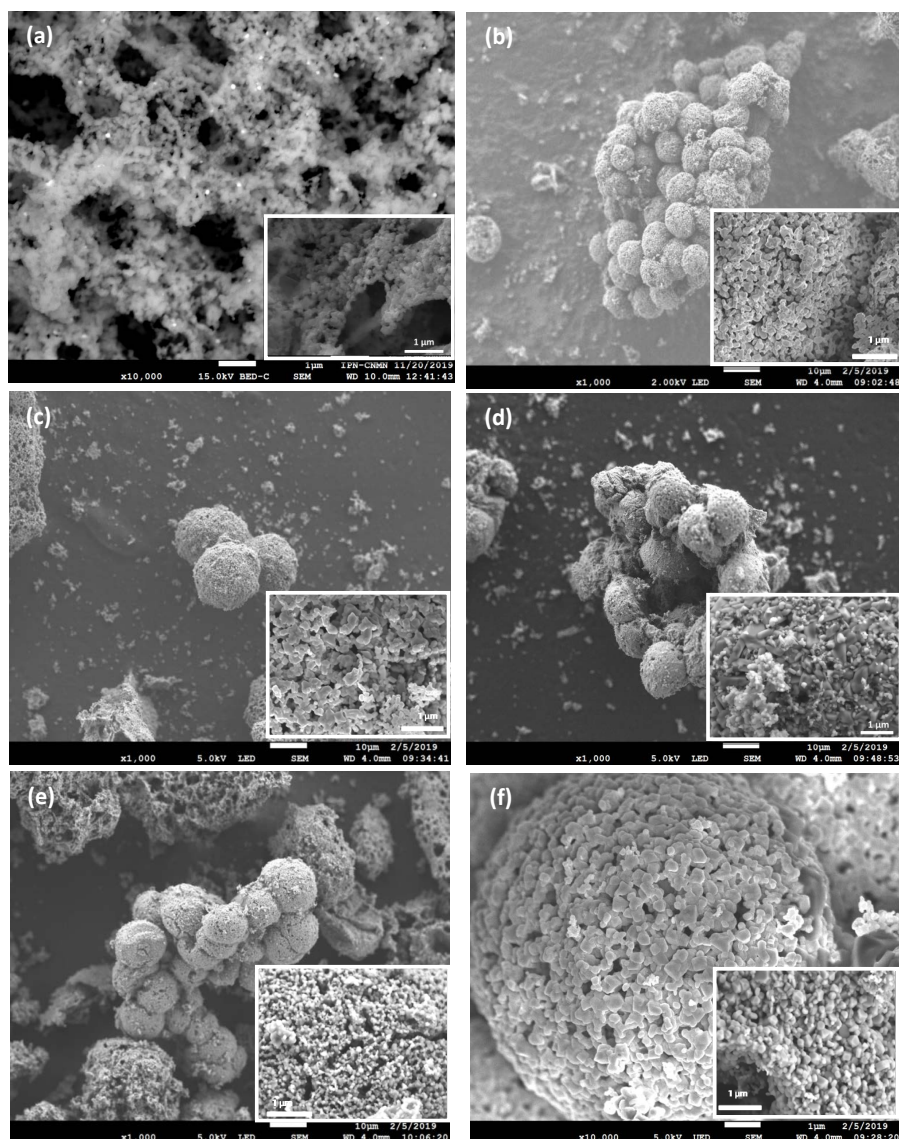


Figure 6. SEM micrographs of the (a) LiCoO_2 , (b) Sm 0.2%, (c) Sm 0.4%, (d) Sm 0.6%, (e) Sm 0.8%, (f) Sm 1% of the $\text{LiCo}_{1-x}\text{Sm}_x\text{O}_y$ powders heat-treated at 700°C .

Figures 6(b)-(f) show the morphologies of the samples containing Sm 0.002, 0.004, 0.006, 0.008, and 0.1 mol%. When these results are compared with those of the non-doped LiCoO_2 powders, it can be seen that the particle size decreases as the concentration of samarium increases. The particle sizes of Sm 0.2%, Sm 0.4%, Sm 0.6%, Sm 0.8% and Sm 1% powders were 126 nm, 123 nm, 122 nm, 121 nm, and 118 nm, respectively.

The TEM images of the Sm 0.4 and Sm 0.8 mol% powders, heat-treated at 700°C , are shown in **Figure 7**. Nanometric particles with an interplanar distance between of 0.22 nm and 0.25 nm can be seen, associated with plane (003). This increase in interplanar distance is the result of the insertion of Sm into the crystalline structure of LiCoO_2 ; as mentioned above, when the proportion of Sm increases, the interplanar distance increases as well.

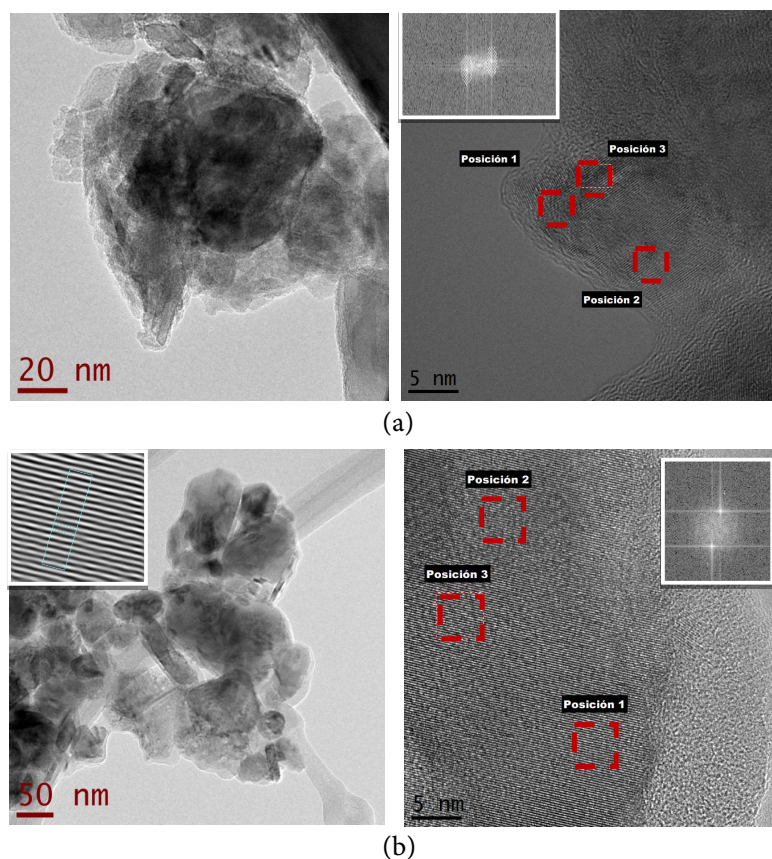


Figure 7. TEM micrographs of the (a) Sm 0.4% and (b) Sm 0.8% powders, heat-treated at 700°C.

4. Conclusions

$\text{LiCo}_{1-x}\text{Sm}_x\text{O}_Y$ -doped powders ($X = 0, 0.002, 0.004, 0.6, 0.008$ and 0.01) were synthesized by the sol-gel method and heat-treated at 700°C. The XRD results confirmed the successful insertion of Sm into the characteristic rhombohedral crystal structure of HT- LiCoO_2 , with no secondary phases. The displacement of the crystallographic planes, specifically in the (003) plane, and the deformation of the unit cell, reflected in an increase in the network parameters, confirm that the doping was successful. The morphology revealed by SEM shows rounded particles that decrease in size from 136 nm to 118 nm as the proportion of Sm decreases.

The integrated intensities ($I(003)/I(004)$) indicate an improvement in the electrochemical properties of the powders (Sm 0.002, 0.004, 0.006, 0.008, and 0.1 mol%) when a value higher than 1.2 is reached. In sum, the powders obtained can be considered candidates for use in cathodes in lithium-ion batteries.

Acknowledgements

The authors gratefully acknowledge the financial support of this work by SIP-IPN projects 20211265 and 20211548 and by CNMN and Lab. CREA C.I.I.TEC. IPN for experimental support. Conacyt project A1-S-28234. Víctor H. Colín

Calderón acknowledges the Conacyt Ms S scholarship. This work was supported by Instituto Politécnico Nacional (Grant N° 31903). The authors also would like to thank Henry Jankiewicz for the editing work that he did for this paper and M. García Murillo for her assistance.

Conflicts of Interest

The authors declare that they have no known competing financial interest or personal relationship that could have appeared to influence the work reported in this paper.

References

- [1] Nishijima, M., *et al.* (2014) Accelerated Discovery of Cathode Materials with Prolonged Cycle Life for Lithium-Ion Battery. *Nature Communications*, **5**, Article No. 4553. <https://doi.org/10.1038/ncomms5553>
- [2] Nitta, N., Wu, F., Lee, J.T. and Yushin, G. (2015) Li-Ion Battery Materials: Present and Future. *Materials Today*, **18**, 252-264. <https://doi.org/10.1016/j.mattod.2014.10.040>
- [3] Ceder, G. (2010) Opportunities and Challenges for First-Principles Materials Design and Applications to Li Battery Materials. *MRS Bulletin*, **35**, 693-701. <https://doi.org/10.1557/mrs2010.681>
- [4] Brog, J.P., *et al.* (2017) Characteristics and Properties of Nano-LiCoO₂ Synthesized by Pre-Organized Single Source Precursors: Li-Ion Diffusivity, Electrochemistry and Biological Assessment. *Journal of Nanobiotechnology*, **15**, Article No. 58. <https://doi.org/10.1186/s12951-017-0292-3>
- [5] Huang, L., *et al.* (2020) Electrode Design for Lithium-Sulfur Batteries: Problems and Solutions. *Advanced Functional Materials*, **30**, Article ID: 1910375.
- [6] Zhang, L., *et al.* (2020) Advanced Matrixes for Binder-Free Nanostructured Electrodes in Lithium-Ion Batteries. *Advanced Functional Materials*, **32**, Article ID: 1908445.
- [7] Yan, C., Yuan, H., Park, H.S. and Huang, J.Q. (2020) Perspective on the Critical Role of Interface for Advanced Batteries. *Journal of Energy Chemistry*, **47**, 217-220. <https://doi.org/10.1016/j.jechem.2019.09.034>
- [8] Li, G.F. and Zhang, J. (2012) Synthesis of Nano-Sized Lithium Cobalt Oxide via a Sol-Gel Method. *Applied Surface Science*, **258**, 7612-7616. <https://doi.org/10.1016/j.apsusc.2012.04.102>
- [9] Yu, X., Sandhu, N.S., Yang, Z. and Zheng, M. (2020) Suitability of Energy Sources for Automotive Application—A Review. *Applied Energy*, **271**, Article ID: 115169. <https://doi.org/10.1016/j.apenergy.2020.115169>
- [10] Gupta, A. and Manthiram, A. (2020) Designing Advanced Lithium-Based Batteries for Low-Temperature Conditions. *Advanced Energy Materials*, **10**, Article ID: 2001972.
- [11] Lockwood, D.J. (2016) *Nanostructure Science and Technology*. Springer, New York.
- [12] Sasmaz, M. (2015) Synthesis and Physical Characterization of Li_xO₂ (X=Ni, Mn, Co, Cu) Nanocomposites for Li Ion Batteries. *Journal of Materials and Electronic Devices*, **1**, 44-49.
- [13] Meng, Y.S. and Arroyo-de Dompablo, M.E. (2013) Recent Advances in First Principles Computational Research of Cathode Materials for Lithium-Ion Batteries. *Accounts of Chemical Research*, **46**, 1171-1180. <https://doi.org/10.1021/ar2002396>

- [14] Ding, Y.H., Zhang, P., Jiang, Y. and Gao, D.S. (2007) Effect of Rare Earth Elements Doping on Structure and Electrochemical Properties of $\text{LiNi}_{1/3}\text{Co}_{1/3}\text{Mn}_{1/3}\text{O}_2$ for Lithium-Ion Battery. *Solid State Ionics*, **178**, 967-971. <https://doi.org/10.1016/j.ssi.2007.04.012>
- [15] Mo, M.Y., *et al.* (2014) Improved Cycling and Rate Performance of Sm-Doped $\text{LiNi}_{0.5}\text{Mn}_{1.5}\text{O}_4$ Cathode Materials for 5V Lithium-Ion Batteries. *Applied Surface Science*, **290**, 412-418. <https://doi.org/10.1016/j.apsusc.2013.11.094>
- [16] Meng, X.D., Han, B., Wang, Y.F. and Nan, J.Y. (2016) Effects of Samarium Doping on the Electrochemical Performance of LiFePO_4/C Cathode Material for Lithium-Ion Batteries. *Ceramics International*, **42**, 2599-2604. <https://doi.org/10.1016/j.ceramint.2015.10.063>
- [17] Yang, W.D., Hsieh, C.Y., Chuang, H.J. and Chen, Y.S. (2010) Preparation and Characterization of Nanometric-Sized LiCoO_2 Cathode Materials for Lithium Batteries by a Novel Sol-Gel Method. *Ceramics International*, **36**, 135-140. <https://doi.org/10.1016/j.ceramint.2009.07.011>
- [18] Aziz, N.A.A., Abdullah, T.K. and Mohamad, A.A. (2016) Synthesis of LiCoO_2 Prepared by Sol-gel Method. *Procedia Chemistry*, **19**, 861-864. <https://doi.org/10.1016/j.proche.2016.03.114>
- [19] Kwon, T., Ohnishi, T., Mitsuishi, K., Ozawa, T.C. and Takada, K. (2015) Synthesis of LiCoO_2 Epitaxial Thin Films Using a Sol-Gel Method. *Journal of Power Sources*, **274**, 417-423. <https://doi.org/10.1016/j.jpowsour.2014.10.070>
- [20] Porthault, H., Baddour-Hadjean, R., Le Cras, F., Bourbon, C. and Franger, S. (2012) Raman Study of the Spinel-to-Layered Phase Transformation in Sol-Gel LiCoO_2 Cathode Powders as a Function of the Post-Annealing Temperature. *Vibrational Spectroscopy*, **62**, 152-158. <https://doi.org/10.1016/j.vibspec.2012.05.004>
- [21] Freitas, B., Siqueira, J., da Costa, L., Ferreira, G. and Resende, J. (2017) Synthesis and Characterization of LiCoO_2 from Different Precursors by Sol-Gel Method. *Journal of the Brazilian Chemical Society*, **28**, 2254-2266. <https://doi.org/10.21577/0103-5053.20170077>
- [22] Soltanmohammad, S. and Asgari, S. (2010) Characterization of LiCoO_2 Nanopowders Produced by Sol-Gel Processing. *Journal of Nanomaterials*, **2010**, Article ID: 104012. <https://doi.org/10.1155/2010/104012>
- [23] Julien, C. (2000) Local Cationic Environment in Lithium Nickel-Cobalt Oxides Used as Cathode Materials for Lithium Batteries. *Solid State Ionics*, **136-137**, 887-896. [https://doi.org/10.1016/S0167-2738\(00\)00503-8](https://doi.org/10.1016/S0167-2738(00)00503-8)
- [24] Satyapal, H.K., Singh, R.K., Sonu Kumar, S. and Bhushan Das, S. (2021) Tuning the Structural, Magnetic and Multiferroic Properties of Sm^{3+} Substituted Barium Hexaferrites $\text{BaFe}_{12-x}\text{Sm}_x\text{O}_{19}$ Nanoceramics. *Materials Today: Proceedings*, **44**, 1833-1840. <https://doi.org/10.1016/j.matpr.2020.12.011>
- [25] Sivaraj, P., Abhilash, K.P., Christopher Selvin, P. and Nalini, B. (2019) Investigations on the Effect Of Sm^{3+} Doping on the Electrochemical Performance of the $\text{Li}_2\text{FeSiO}_4/\text{C}$ Nanocomposite Cathode Material for Lithium Ion Batteries. *Materials Today: Proceedings*, **8**, 346-351. <https://doi.org/10.1016/j.matpr.2019.02.121>
- [26] Reddy, M.V., *et al.* (2014) Studies on Bare and Mg-Doped LiCoO_2 as a Cathode Material for Lithium-Ion Batteries. *Electrochimica Acta*, **128**, 192-197. <https://doi.org/10.1016/j.electacta.2013.10.192>
- [27] Huang, B., Wang, M., Zuo, Y.X., Zhao, Z.Y., Zhang, X.W. and Gu, Y.J. (2020) The Effects of Reheating Process on the Electrochemical Properties of Single Crystal $\text{LiNi}_{0.6}\text{Mn}_{0.2}\text{Co}_{0.2}\text{O}_2$. *Solid State Ionics*, **345**, Article ID: 115200. <https://doi.org/10.1016/j.ssi.2019.115200>

- [28] Yuan, H., Song, W.B., Wang, M., Gu, Y.J. and Chen, Y.B. (2019) Lithium-Ion Conductive Coating Layer on Nickel Rich Layered Oxide Cathode Material with Improved Electrochemical Properties for Li-Ion Battery. *Journal of Alloys and Compounds*, **784**, 1311-1322. <https://doi.org/10.1016/j.jallcom.2019.01.072>
- [29] Wu, Q., Li, W.R., Cheng, Y. and Jiang, Z.Y. (2005) Homogenous LiCoO₂ Nanoparticles Prepared Using Surfactant P123 as Template and Its Application to Manufacturing Ultra-Thin-Film Electrode. *Materials Chemistry and Physics*, **91**, 463-467. <https://doi.org/10.1016/j.matchemphys.2004.12.011>
- [30] Muniz, F.T.L., Miranda, M.A.R., Morilla dos Santos, C. and Sasaki, J.M. (2016) The Scherrer Equation and the Dynamical Theory of X-Ray Diffraction. *Acta Crystallographica Section A: Foundations and Advances*, **72**, 385-390. <https://doi.org/10.1107/S205327331600365X>
- [31] Ingham, B. and Toney, M.F. (2014) X-Ray Diffraction for Characterizing Metallic Films. In: Barmak, K. and Coffey, K., Eds., *Metallic Films for Electronic, Optical and Magnetic Applications*, Woodhead Publishing, Cambridge, 3-38. <https://doi.org/10.1533/9780857096296.1.3>